Improving the accuracy of clipless eye positioning with Kappa-Angle calibration and surface imaging

Saturday, 1 June 2024

Semester Project Report - Marina Crespo Aguirre

Supervisor Prof. Dr. Antony John Lomax

Advisors : Dr. Riccardo Via, Dr. Giovanni Fattori

PAUL SCHERRER INSTITUT
PSI

ETH

INDEX

1. INTRODUCTION

Tumours of the choroid, ciliary body and iris of the eye, known as uveal melanomas represent a common type of intraocular tumours, with an incidence of 6 per million cases every year in Western Countries [1]. Due to their asymptomatic nature, early diagnosis and treatment are key for the clinical management of ocular patients, preventing the development of distant metastasis [2]. Common therapeutic options for this indication are brachytherapy and external beam radiotherapy which allow for organ retention and, if possible, preserve vision.

Ocular Proton Therapy (OPT), a refined form of external beam radiotherapy that makes use of proton beams, is the gold standard treatment for peripapillary ocular melanomas, reporting high level of tumour control and eye preservation. This treatment has proven to be extremely effective with local control rates well over 90%, reported by several institutions [2,3,4]. Thus current research effort is focused towards improving the workflow to minimise the invasiveness of the treatment and integration of multi-modal imaging for better definition of the treatment geometry.

The conventional OPT treatment relies on a geometric model of the eye scaled to the individual patient. This technique commonly requires the surgical implantation of tantalum marker (clips), which are sutured to the outer surface of the eye and are used to localize precisely the intra-ocular tumours [4]. Following surgical implantation, a treatment simulation session takes place in the radiotherapy bunker. There, the three-dimensional position of the clips is measured with calibrated orthogonal X-ray imaging. These in-room radiographies, combined with the annotations of the surgeon and ophthalmologist, and ancillary imaging like ultrasound and fundus photography, allow the definition of a geometrical model for treatment planning, the most known software used for this purpose being EyePlan [5]. Figure 1 shows the components and output of the geometric model of the eye using this software.

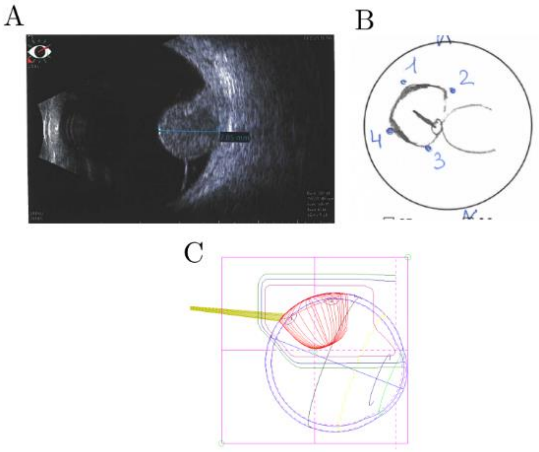

Figure 1. EyePlan modelling pipeline. A. Ultrasound scan including tumour depth information. B. Annotations from ophthalmologist on clips positions. C. EyePlan Geometric fitting.

From such eye model, a treatment plan is optimised, defining the orientation of the eye that best allows the proton beams to reach the tumour whilst avoiding dose deposition to critical structures in each individual patient. After eye modelling and treatment planning and before treatment delivery a geometry verification session takes place. Here, several radiographies of the eye are taken, verifying for the correct alignment of the eye with respect to planned position, by point-based registration of clips positions. This is done iteratively, aiming for the optimal gaze direction that brings the patient's clips, and in turn the tumour, to be as close as possible within the reference plan [3].

Then, the treatments take place, commonly performed in four sessions on consecutive days. The protons are delivered via a fixed horizontal beam. Energy, maximal penetration depth and cross-sectional shape of the beam can be individually modified to the need of each patient, with the help of collimators specifically fabricated. Figure 2 illustrates a schematic of the OPTIS2 treatment room geometry, which includes a moving chair, and a mask holder where the patient's head will be fixed.Figure 2

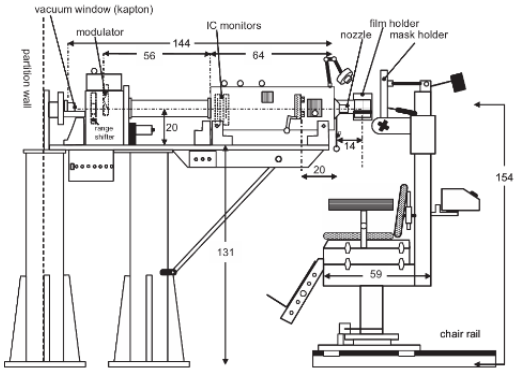

Figure 2. OPTIS beamline.

The challenges related to this conventional technique, namely the invasiveness and heavy reliance on the surgeon's expertise for clips' implantation, have motivated the investigation of non-invasive alternatives for eye localization. A novel proposal by Via et al. focuses on real-time, three-dimensional target localization using optical eye tracking techniques and fringe pattern profilometry. Such technique relies on an optical Eye Tracking System (ETS) which comprises multiple calibrated cameras to triangulate the real-time position of the eye pupil [6] [7] and synchronised projectors to enable 3D measurement of the cornea-scleral surface, based on the analysis of the deformation of a Ronchi pattern onto a fraction of the oriented eye, captured with the cameras [8].

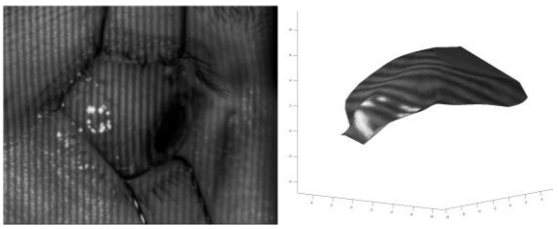

Figure 3. Optical tracking of the eye through fringe pattern profilometry [Via et al]. On the left, projection of pattern. On the right 3D reconstruction of the sclera.

This novel approach has potential for clinical translation of clip-less OPT. However, some limitations and simplifications in the underpinning geometrical model, need to be further investigated. In fact, in such original proposal, the eye localisation is based on the 3D pupil position and the anterior surface of the oriented eye to identify the gaze direction, and based on that, computing the patient position correction required to align the tumour. At the current state of development, this technique assumes a perfect alignment between the symmetry axis of the eye and the gaze direction or visual axis, an oversimplification of the geometric model that might lead to errors in eye positioning, and thus suboptimal delivery of the hypothetical proton therapy, when the beam-patient relative position is not exactly matching the planned treatment geometry.

The eye model definition allows the tumour localisation from the optical imaging of the anterior eye segment, and is therefore crucial in such positioning approach. The widely used EyePlan eye model, known to be robust, but also giving a simple approximation of the patient eye, is recently being replaced by modern treatment planning systems, that base the geometry definition on volumetric diagnostic imaging (Computer Tomography, CT, and Magnetic Resonance Imaging, MRi) rather than solely on intra-operative surgical measurements of eye length and clips position.

In this project, we use the eye model implemented in RayStation RayOcular v.14.0 treatment planning system [9], that supports CT and MRI based fitting of the eye geometrical components (see Figure 4). In particular, and importantly for gaze estimation, it enables the definition of the "macula", a region close to the optic disk where a high density of cone cells is located, that is commonly associated with the gaze or visual axis [10].

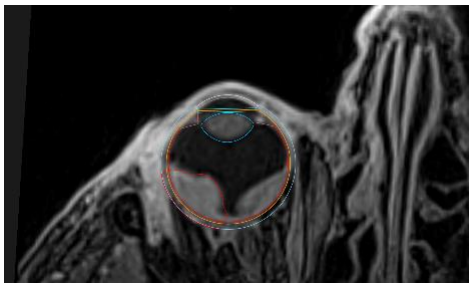

Figure 4. Eye model from RayOcular software overlapped to MRI acquisition.

Identifying the macula location is however non-trivial due to its dimension and the limited resolution of CT and MRI. In a previous study, it has been shown how fundus photography, a modality commonly used to capture the interior part of the eye, can be registered to the MRI scans for improving the modelling of the tumour volume [11]. Based on MRI-Fundus imaging registration, a patient-specific macula can be therefore obtained, leading to more accurate definitions of the gaze direction, which could have considerable effects when implemented on the clip-less technique of eye positioning.

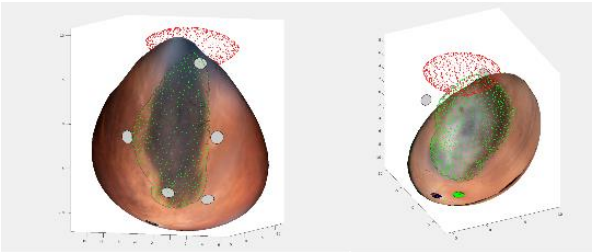

Figure 5. MRI-Fundus registration example results.

This semester project focuses on this clipless eye-tracking techniques, aiming to improve them. For this reason, some physiological parameters related to the angle between the visual and optical axis, the so-called 'kappa angle', have been explored. We hypothesize that by calibrating for this angle the registration, a more robust estimation of the patient-specific gaze direction will be understood.

Through this higher precision modelling, a better eye positioning without the need of clips will be derived, hypothesized to be as good as the conventional technique, without the need of iterative repositioning in the geometry verification stage. This way, in the geometry verification, the fixation light position would be resolved, and the optimal eye orientation for the treatment would be estimated.

Structure and Objectives

The structure followed in this report to introduce the concepts investigated begins with a first part that presents the mathematical convention used to model the kappa-angle between visual and optical axes in different patients. A validation of the convention is then performed, comparing the results from two sessions, the treatment simulation and a treatment fraction.

The second part of this study focuses on exploring different strategies of clip-less eye registration. For this, the kappa angles modelled in the previous part will be used and integrated to the proposed methods of registration, evaluating the error in positioning by comparing the clip-based tumour location with the registration results.

2. MATERIALS

The dataset used in this project comes from a prospective study for imaging scleral topography and pupil position in patients undergoing ocular proton therapy within the frame of the EKNZ 2019-01987, approved by the ethics committee Ethikkommission Nordwest- und Zentralschweiz. Four patients were selected out of this clinical database.

For each patient, the dataset includes:

- The geometrical eye model defined in RayOcular TPS.

And, for every X-ray acquisition from two sessions, corresponding to the treatment simulation and the treatment fraction, the dataset includes as well:

- The reference positions of the eye clips
- The fixation light position, towards which the patient was instructed to look.
- Three-dimensional surfaces of the scleral-cornea segment of the eye reconstructed with fringe pattern profilometry
- The position of the pupil estimated with the eye tracking system.

All data processing was carried out in Python v 3.11.7, and Inkscape v 1.3.2 was used to generate the figures.

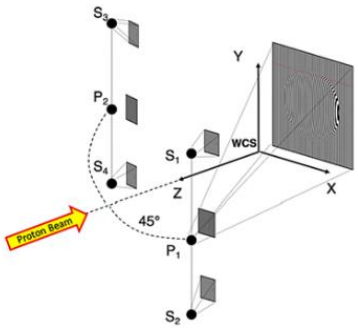

Figure 7. Representation of the system introduced in OPTIS for 3D reconstruction of the pupil and eye surface.

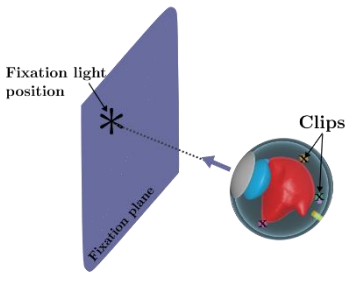

Figure 6. Illustration of the eye model and the reference positions of the clips and fixation light.

3. METHODS

Eye movements are described by a set of three rotations, around cardinal axes X, Y and Z; and a translation vector. The transformations are performed in a local, eye-mounted, frame of reference (Fick coordinate system), with origin at the centre of the eyeball. The treatment room coordinate system (RCS) on the other hand, is aligned to the iso-centre of the proton beam.

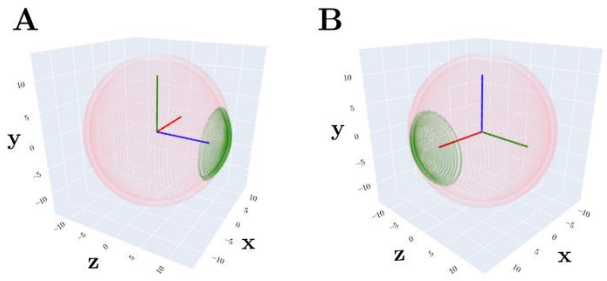

Figure 8. Reference system convention. A. Eye model in room coordinate system. B. Eye model in Fick coordinate system

Composing the eye rotations follows the Fick-Gimbal convention [12], where the eye position is characterized by a rotation φ (azimuthal angle) about the vertical axis, followed by a rotation θ (polar angle) around the horizontal axis and a rotation ϕ (torsion angle) around the line of sight.

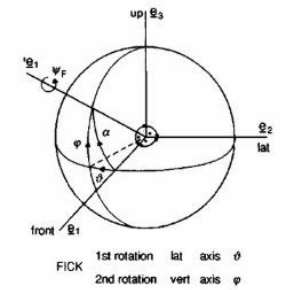

Figure 9. Eye rotations in Fick convention

Eye transformations are therefore described as follows:

1. Move from the RCS to the Fick system using the following equations:

$$R_{RCS\rightarrow Fick} = R_{\varphi} \cdot R_{\theta} \cdot R_{\phi};$$

where $\varphi = \phi = 90º$, and $\theta = 0º$

$$R_{\phi} = \begin{bmatrix} 1 & 0 & 0 \\ 0 & \cos(90º) & -\sin(90º) \\ 0 & \sin(90º) & \cos(90º) \end{bmatrix}; R_{\theta} = \begin{bmatrix} \cos(0) & 0 & -\sin(0) \\ 0 & 1 & 0 \\ \sin(0) & 0 & \cos(0) \end{bmatrix}; R_{\varphi} = \begin{bmatrix} \cos(90º) & -\sin(90º) & 0 \\ \sin(90º) & \cos(90º) & 0 \\ 0 & 0 & 1 \end{bmatrix}$$

2. Once in Fick system of reference, the following transformation matrix describes the rotations and translations needed to register an object from position B to position A:

$$T_B^{B\prime} = \left[\begin{array}{ccc|c} & R_B^{B\prime} & & P_B^{B\prime} \\ \hline 0 & 0 & 0 & 1 \end{array}\right]$$

Where $R_B^{B\prime} = R_x \cdot R_y \cdot R_z$ corresponds to the rotation around the origin, and P corresponds to the translation vector.

Note that: $R_x = \begin{bmatrix} \cos(\varphi) & -\sin(\varphi) & 0 \\ \sin(\varphi) & \cos(\varphi) & 0 \\ 0 & 0 & 1 \end{bmatrix}$, $R_y = \begin{bmatrix} \cos(\theta) & 0 & -\sin(\theta) \\ 0 & 1 & 0 \\ \sin(\theta) & 0 & \cos(\theta) \end{bmatrix}$, and $R_z = \begin{bmatrix} 1 & 0 & 0 \\ 0 & \cos(\phi) & -\sin(\phi) \\ 0 & \sin(\phi) & \cos(\phi) \end{bmatrix}$

In summary, in order to simulate geometric transformations of the eye, the following computations are needed:

- $RCS \rightarrow Fick$ coordinate system mapping: $P^B_{[Fick]} = T^{[Fick]}_{[RCS]} \cdot P^B_{[RCS]}$
- Registration operation: $P^{B\prime}_{[Fick]} = T^{B\prime}_B \cdot P^B_{[Fick]}$
- $Fick \rightarrow RCS$ coordinate system mapping: $P^{B\prime}_{[RCS]} = T^R_{[Fick]} \cdot P^{B\prime}_{[Fick]}$

Part 1. The Kappa angle

There are two significant axes in the eye; the *optical axis*, which corresponds to the line passing through the centre of the eyeball and the cornea, and the *visual axis*, line passing through the cornea centre and intersecting the sclera in the fovea, i.e. the midpoint of the so-called macula.

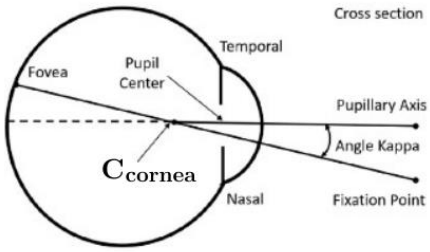

Figure 10. Schematics of the eye

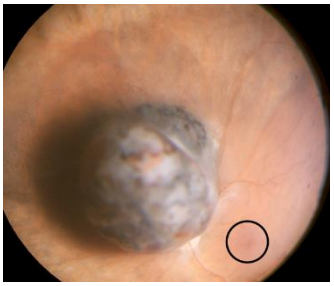

Figure 11. Fundus photograph with marked macula in shaded region

The visual axis is assumed to be pointing at the fixation point, i.e. the fixation light position in the treatment room. Based on that, the visual axis could be estimated based on clips points registration for each eye orientation, as the line back-traced from the fixation light position and passing through the cornea curvature center of the eye model.

Given the clips reference positions in RCS, least squares points registration (Kabsch algorithm) was used to solve the rigid transform analytically, computing the rotations and translations required to replicate the eye position the patient was assuming in every acquisition.

Point-based registration starts with the estimate of the centroids of the two datasets to register. Then, the algorithm centres the centroids at the origin and estimates the rotation required that best align the points. The rotations are applied to one set of centroids, and the translations needed to register both cloud of points is estimated.

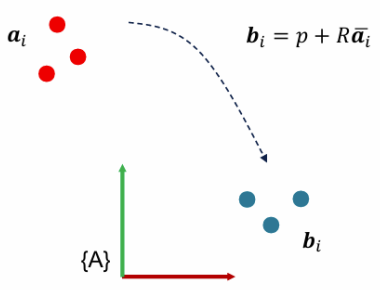

Figure 12. Kabsch algorithm. Point-based registration

The steps can be summarized :

1. $\bar{a} = \frac{1}{N}\sum_{i=1}^{N}\overrightarrow{a_i}$, $\bar{b} = \frac{1}{N}\sum_{i=1}^{N}\overrightarrow{b_i}$
2. $\widetilde{a_i} = \overrightarrow{a_i} - \bar{a}$, $\widetilde{b_i} = \overrightarrow{b_i} - \bar{b}$
3. $H = \widetilde{\boldsymbol{A^T}} \cdot \widetilde{\boldsymbol{B}}$; $H = U\Sigma V^T$; $\boldsymbol{R} = V \cdot U^T$ – rotation matrix
4. $\boldsymbol{t} = \bar{a} - R\bar{b}$ – translation vector

In this way, the eye position relative to the room coordinate is defined for each acquisition and the macula position can be computed casting a ray from the light position, though the eye model. We refer to this as the 'clip-based' macula position, and it's assumed to be the best guess or ground truth for comparison with other models.

More in detail, once the eye was oriented, the position of the fovea was estimated by back tracing the visual axis to intersect the posterior segment of the eyeball. Note that the intersection of the axis with the sclera, given as a scattered point cloud, was obtained indirectly, as we could not get a line to surface intersection. The estimated intersection, comes from the weighted average of the points in the sclera within a maximum distance to the visual axis of 1mm as follow:

$$fov = \frac{1}{N}\sum_{i=1}^{N}\frac{1}{d_i}\cdot\overrightarrow{p_i}$$

$$where\ d_i = |\overrightarrow{p_i} - \overrightarrow{v_{axis}}|\ ; \qquad and\ 0 \leq\ d_i \leq 1\ [mm]$$

Once the fovea is identified in RCS, a mapping to Fick coordinate system is required to move on local eye frame of reference and define the kappa angle. In doing that, the fovea position is expressed in spherical coordinates, as azimuthal and elevation angle rotations around the Z and X axis.

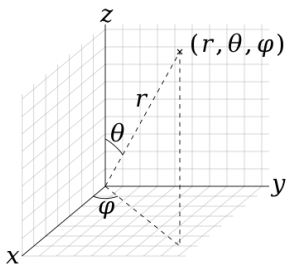

Figure 13. Spherical coordinates

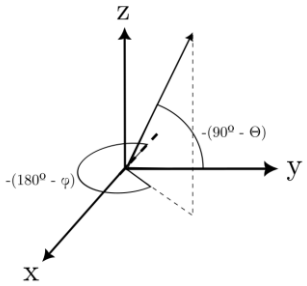

Figure 14. Representation of the adjustment required to derive the kappa angle out of the fovea coordinates

An adjustment of the spherical coordinates of the Fovea is needed to calculate the kappa angle components, this is illustrated in Figure 14 where:

$$\varphi_k = -(180º - \varphi) \text{ and } \vartheta_k = -(90º - \vartheta)$$

The consistency of such estimate of the kappa angles estimation was validated by comparing its median value across all acquisitions for all patients. To test the robustness of the modelling, we used non-parametric Mann Whitney U-test, given the small dimension of the dataset, which was not normally distributed.

Such nominal macula position has been compared with two alternative estimates:

1. A pre-defined fovea position in available the RayOcular eye models set at zero degrees elevation and four degrees of azimuthal angle to the left or to the right of the symmetry axis, depending on whether it is a left or right eye.
2. The macula definition coming from the MRI-Fundus registration. In this case, we set the fovea position at center of mass of the scatter of points composing the macula structure.

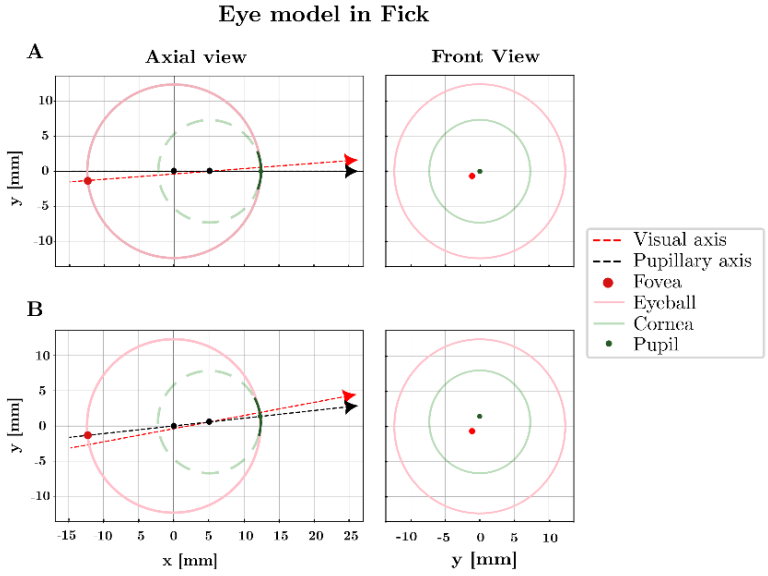

Figure 15. Kappa angle geometrical validation. A. Initial position of the eye, in red the visual axis, in black the optical axis. B. Visualization of the eye rotated with the kappa angles.

In this comparative analysis kappa values obtained with the different fovea definitions were analysed. Note that clips-based kappa values come from computing the median angles obtained from the two sessions including several gaze angles, and therefore can be considered more accurate than the MRI-Fundus registration which is based on a single measurement.

The comparison is based on the analysis of the fixation point recalculated by back projecting the visual axis from each different fovea positions, to intersect with the fixation plane. We hypothesize that the more generic the fovea definitions, the greater the error in fixation light estimated position.

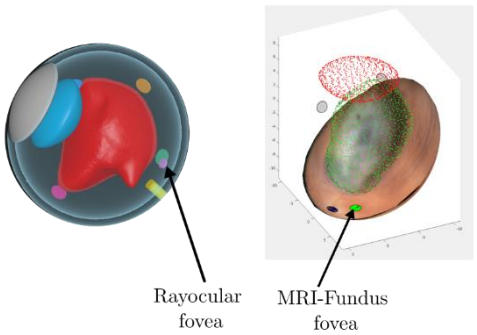

Figure 16. Fovea definitions from the Rayocular software and the MRI-Fundus registration

Part 2. Clipless eye positioning with non-invasive optical measurements

The second part of this study focuses on the clip-less eye positioning, from the pupil position and scleral surface measured with the cameras and the pattern projections.

In the previous studies, the algorithm was based on registering the sclera of the geometric eye model to the points in the surface, making use of Iterative Closest Points algorithm and the three-dimensional pupil position measured with the ETS. The approach taken in this study makes use of a modified version of the ICP and includes a revision of the pupil position information for improved registration accuracy.

Pre-processing of Scleral topography

The reconstructed eye surface from pattern profilometry projection, is characterized by a high resolution and therefore very closely distanced points, in some cases, noisy regions are observed Figure 17. As a pre-processing step, KD trees were used to discard possible outliers.

Points of the surface were considered outliers when their distances to the closest points were greater than 0.2 mm. A KD-tree is a data structure used for organizing points in a k-dimensional space, and it is particularly useful to solve tasks in multidimensional search keys such as nearest neighbours.

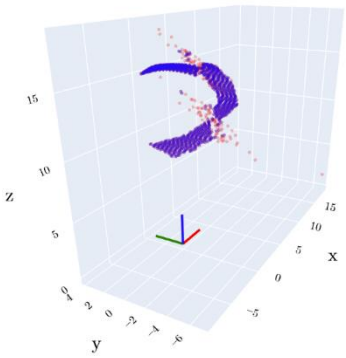

Figure 17. Figure 16. Denoising the scleral topography, in blue the denoised version of the original surface represented in red

In a k-d tree, each node represents a k-dimensional point, specifying as well a splitting dimension, which cycles through the dimensions as one goes down the tree. This way, when a new point is introduced into the tree, its nearest neighbours in k dimensions are easily identified.

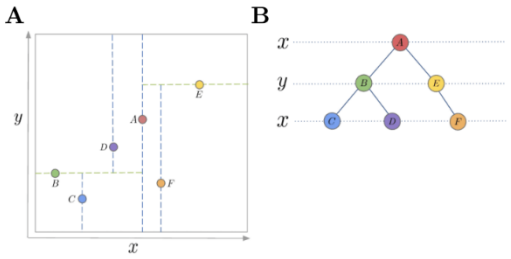

Figure 18. KD tree. A. Visualization of the structuring process in KD tree. B. Representation of iterative process behind the computation of a KD tree

Iterative Closest Points

After pre-processing, the geometric eye model is registered to the measured 3D surface of the oriented eye, by minimizing the distance between corresponding points. The correspondences are newly established at every iteration making use of KD trees.

In this context, the k-d tree is built from the sclera of the eye, organizing the points into a binary structure, where each node splits the space into two half spaces. Then, a query is done to find the closest single point in the surface to the sclera. The algorithm traverses the KD tree from root to leaves, at each node choosing the branch that is closest to the query point. Once a leaf node is reached, the algorithm backtracks, checking other branches in case they might contain closer points, and ensuring that the closest point is found efficiently.

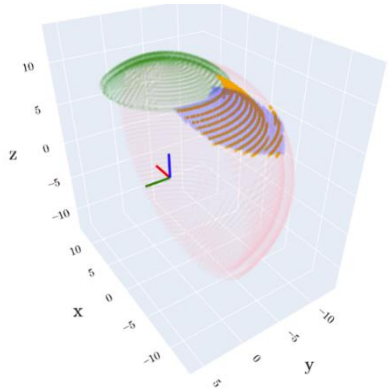

Figure 19. 3D rendering of the eye, displaying in blue, the oriented surface to align the model with, in orange the corresponding closest points in the sclera.

Once the correspondences surface-sclera have been identified, and their distances to their closest single point are known, a minimization function based on the 'L-BFGS-B' method (for Limited-memory Broyden-Fletcher-Goldfarb-Shanno with Box constraints) is used to compute the optimal orientation of the sclera. The algorithm would find the x that minimizes the value of $f(x)$;

$$f(x) = \frac{1}{N}\sqrt{\sum_{i=j=1}^{N}(p_i - p_j)^2}$$

Where x is the vector of transformation parameters in $\mathbb{R}^5$, which contains the azimuthal (θ) and elevational (φ) angle rotations, as well as the three translations in x, y and z, to be iteratively introduced to move the eye until an optimal combination of the parameters is found. Note that the third rotation component, i.e. the torsional rotation, is computed out of the two other rotation angles with the following formula [13]:

$$\psi = \frac{\sin(\theta)\sin(\varphi)}{1 + \cos(\theta)\cos(\varphi)}$$

In order to optimize search of the best x, a set of constraints are introduced into the algorithm for its regularization.

Constraint 1. Pupil

The ETS-measured pupil position in 3D is used as first registration constraint. A modified version of the optimization algorithm includes the point-to-point distance minimization of the pupil in the geometric model, defined as the intersection of the optical axis with the anterior part of the cornea, with respect to the measured reference (see Figure 20).

At every iteration, the model is transformed and the associated pupil position updated based on current registration parameters.

$$\lambda_1 = \left|\vec{p}_{ref} - \vec{p}_{it}\right|$$

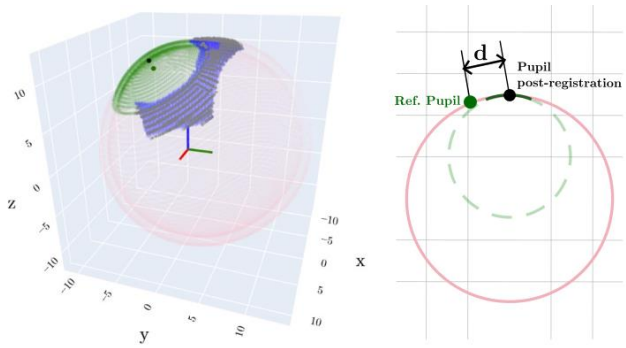

Figure 20. Illustration of the pupil constraint. Left figure, rendering of the eye with the surface mounted onto the sclera and the two definitions of the pupil. Right, schematics of the pupil regularizer.

Constraint 2. Optical axis

An alternative approach to make best use of the pupil reference position, is based on minimizing the angle between the reference optical axis (estimated from the reference pupil position and the center of the eye model), and the optical axis resulting from the iterative re-positioning of the estimated pupil. Both axes intersect in the center of the cornea, therefore the constraint metric becomes:

$$\lambda_2 = \arccos\left(\frac{(\vec{o}_{ref} \cdot \vec{o}_{it})}{\|\vec{o}_{ref}\|\|\vec{o}_{it}\|}\right)$$

Where $\vec{o}_{ref}$ and $\vec{o}_{it}$ are the direction vectors of the reference optical axis and the optical axis obtained in each iteration respectively.

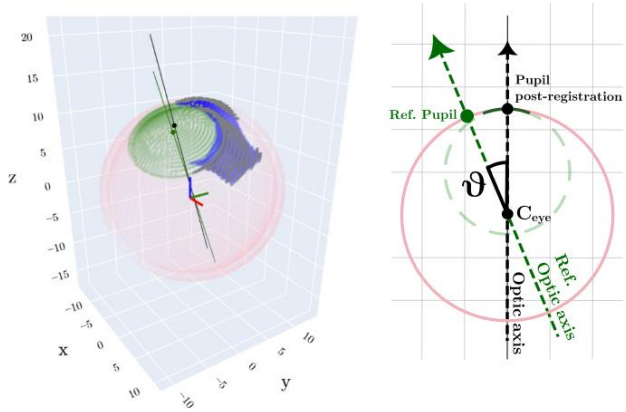

Figure 21. Illustration of the optical axis constraint. Left image corresponds to the rendering of the eye model with the aligned optical axes. On the right, a schematic representation of the optic axis regularizer

Constraint 3. Visual axis

The last constraint considered for the optimisation of x is based on the inclusion of the kappa angle parameter estimated in the previous part of this study. As mentioned before, if the kappas are known, the gaze direction can be computed, and an estimate of the patient-specific fovea can be derived accordingly. In order to make use of these concepts, we define another constraint of the surface registration based on minimizing the angle between the visual axis computed in each iteration (line passing through the reference fixation light position and the centre of the cornea in the model), and the reference visual axis (line passing through the estimated fovea and the centre of the cornea in the model), see Figure 22.

$$\lambda_3 = \arccos\left(\frac{(\vec{v}_{ref} \cdot \vec{v}_{it})}{\|\vec{v}_{ref}\|\|\vec{v}_{it}\|}\right)$$

where $\vec{v}_{ref}$ and $\vec{v}_{it}$ are the direction vectors of the reference visual axis and the visual axis obtained in each iteration respectively.

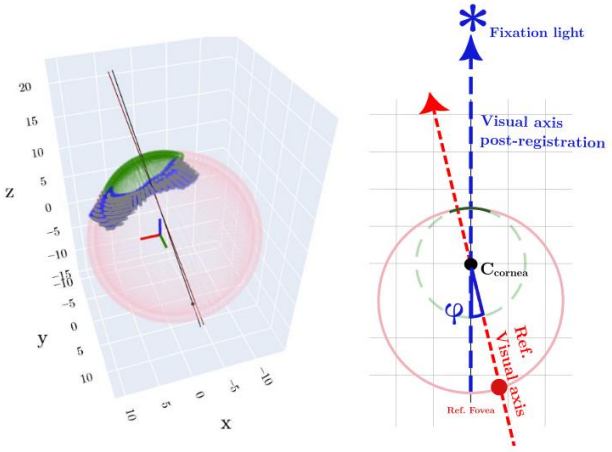

Figure 22. Illustration of visual constraint. On the left, rendering of the eye with the aligned visual axes. On the right, schematic representation of the visual axis regularizer

In this way, the final expression for the function to be minimized $f(x)$ becomes:

$$\frac{1}{N}\sqrt{\sum_{i=j=1}^{N}(p_i - p_j)^2} + b \cdot \lambda$$

where $\lambda = \lambda_1, \lambda_2, \lambda_3$, and b is a parameter that controls the weight of the regularizer with respect to the surface minimization component.

To validate the robustness of the proposed constraints, a combination of the different regularizers is studied. We define three sets of functions of increasing complexity to be optimized:

$$f_1(x) = \frac{1}{N}\sqrt{\sum_{i=j=1}^{N}(p_i - p_j)^2} + b \cdot \lambda_1$$

$$f_2(x) = \frac{1}{N}\sqrt{\sum_{i=j=1}^{N}(p_i - p_j)^2} + b \cdot \lambda_2$$

$$f_3(x) = \frac{1}{N}\sqrt{\sum_{i=j=1}^{N}(p_i - p_j)^2} + b \cdot \lambda_2 + c \cdot \lambda_3$$

The analysis is based on the comparison of the registration metric at convergence, as well as the error in tumor position resulting from the three approaches introduced. The tumor position error is defined as the delta between the center of mass of the tumor volume obtained with the different registration methods, with respect to the center of mass of the tumor registered with the clips reference positions:

$$\vec{e_i} = \sqrt{\left(\overrightarrow{cT_{ref}} - \overrightarrow{cT_i}\right)^2}\,.$$

We obtain an error vector whose x, y and z components will be analyzed individually. Our hypothesis is that the best method will be the one with the largest number of constraints $f_3(x)$.

In a second analysis, we investigated the effect of the different kappa angles' definitions on the registration results using the cost function $f_3(x)$, the one that considers the visual axis to perform the alignment. We again used the same metric to estimate the deviation in tumor positioning with respect to the clips-based reference.

We compare kappa values, and thus the macula position definition, coming from the Ray Ocular model, MRI-Fundus registration, and the patient-specific calibration described in the first section of this report. Our hypothesis is that similarly to the previous part, more accurate kappas will lead to better registration results, and therefore smaller tumor deviations in positioning. Kappas from clip-based registration are expected to be the best estimation amongst the three.

The statistical test used to quantify the intra-method robustness, and intra-kappa accuracy, is Mann Whitney U-test at a confidence level of 5%.

5. RESULTS

Part 1. Kappa angle

The results for the kappa angles analysis for the entire dataset are presented in Figure 24, Error! Reference source not found. and Table 1. No significant correlation was found between the values of polar an azimuthal kappa angles within session of the same patient. Of note for some patients, the azimuthal component of the kappa angle is positive while in others it is negative. Error! Reference source not found. illustrates a frontal view of the positions of the fovea in all patients, calculated by back projection of the visual axis from the fixation light position, colour coded to represent the different acquisitions.

The accuracy of patient specific kappa values was quantified by evaluating the fixation point position, when using different definitions of kappa, with respect to the reference positions. Figure 23 illustrates in polar plots, a particular case of a patient. The scatter of points corresponds to the errors in polar

coordinates with respect to the reference (centred at the origin), colour coded to represent the different acquisitions.

An increasing variance of the error associated with decreasing level of specificity in the kappa angle definition can be visually appreciated. As expected, in the case of the clip-based kappa values, assumed to be perfectly modelling the optical-visual axis deviation, the scatter of points is clustered around the origin.

	Simulation		Fraction 1	
	φ [deg]	ϑ [deg]	Δφ [deg]	Δϑ [deg]
Patient 1	4.0461	6.7813	3.42925	0.9432
Patient 2	-9.31	3.42125	0.5724	0.3271
Patient 3	5.96565	-0.94925	0.82525	0.78065
Patient 4	-5.2547	5.2994	0.4658	4.298

Table 1. Median of kappa angles [azi, polar] for the different patients with their corresponding inter-session deviation.

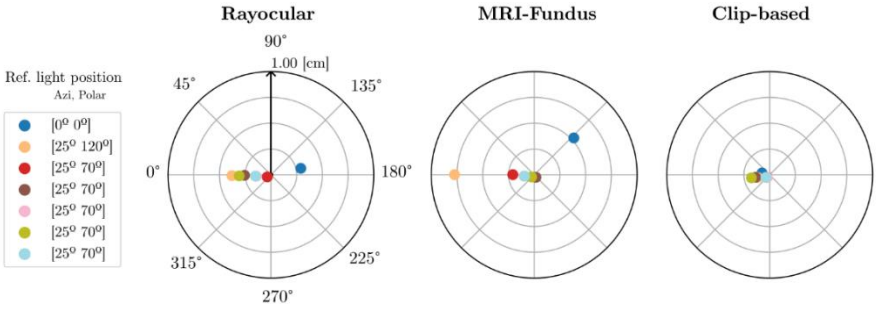

Figure 23. Fixation light re-estimation from the three definitions of the fovea, Rayocular model, MRI-Fundus registration and Clip-based estimation.

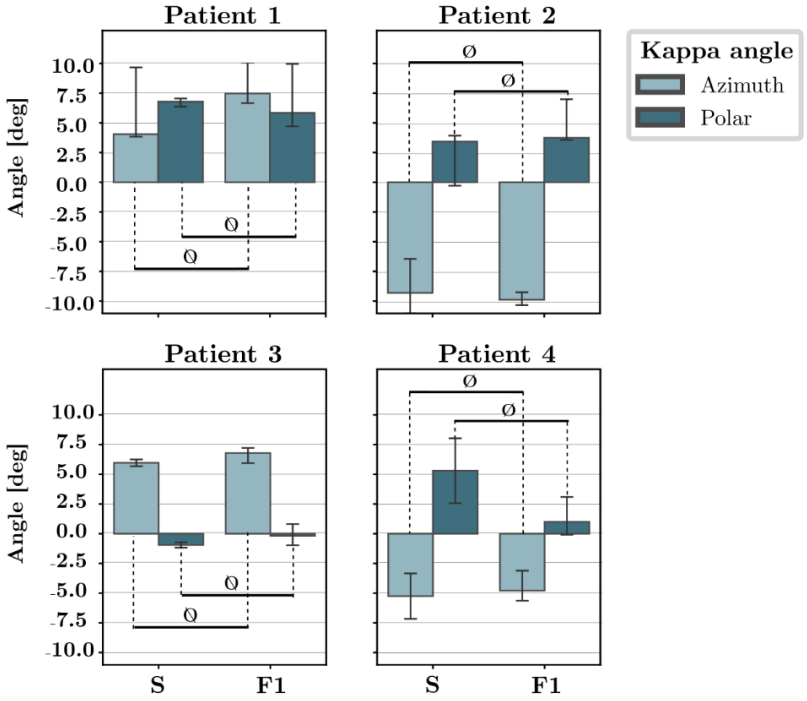

Figure 24. Bar plots of the medians of kappa angles and interquartile range of the four patients for simulation (S) and first fraction (F1) of the treatment

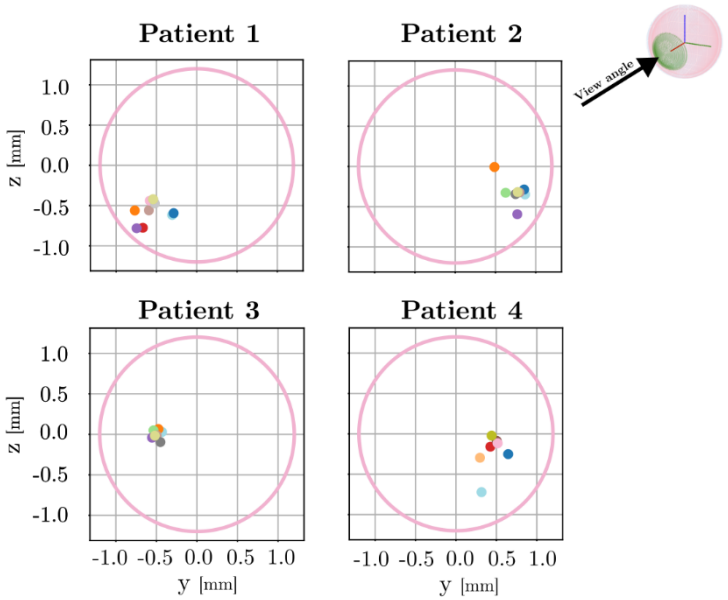

Figure 25. Frontal view of the normalized eyeglobe with the clip-based foveas colour coded for the different acquisitions.

Part 2. Surface Registration

The results from the second part of the study are represented in Figure 26, Table 2, and Figure 28, Table 3.

In Figure 26, the error components in x, y and z coordinates, with respect to the reference positions of the tumour centre of mass, can be observed. The median values of the error in registration from all methods are also displayed in table 2. Significant differences between the differently constrained registration methods have been observed, with Visual method showing the best results

Tumour positioning error			
Method	**Median of error components**		
	x [mm]	**y [mm]**	**z [mm]**
Pupil	2.396	2.864	0.984
Optic	1.436	1.984	1.67
Visual	0.791	1.032	1.51

Table 2. Median of errors in tumour positioning based on the three methods of registration.

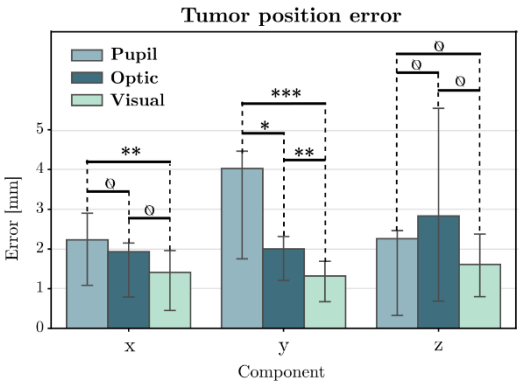

Figure 26. Median and interquartile range of registration errors for the three methods of registration evaluated.

Figure 27 depicts the 3D volumetric representation of the treatment target volume localised with clips (in green) and with clipless eye registration (in red) for one exemplary patient using the three different registration methos, One can observe an increasing overlap between the reference tumour position and the resulting tumour after non/invasive eye localisation.

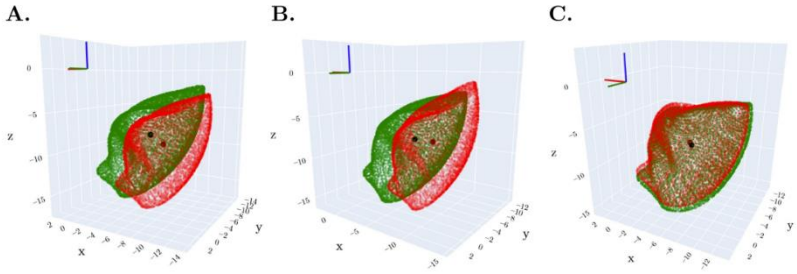

Figure 27. Overlap between ground truth tumour (in green) and tumour post-registration (in red).

Finally, the discrepancy in tumour position estimation with respect to clips measurement, based on the three different kappas definition, can be observed in Figure 28, and the median of error components summarized in table 3. Here, even though the magnitude of the error in all the components was qualitatively smaller when using the clip-based kappas (see Table 3), no statistically significant difference was found using the Mann-Whitney U test.

Tumour positioning error			
Kappas	**Median of error components**		
	x [mm]	**y [mm]**	**z [mm]**
RayOcular	0.842	1.442	1.732
MRI-Fundus	0.603	1.438	1.944
Clip-based	0.791	1.032	1.51

Table 3. Median of errors in tumour registration based on the three different kappa definitions

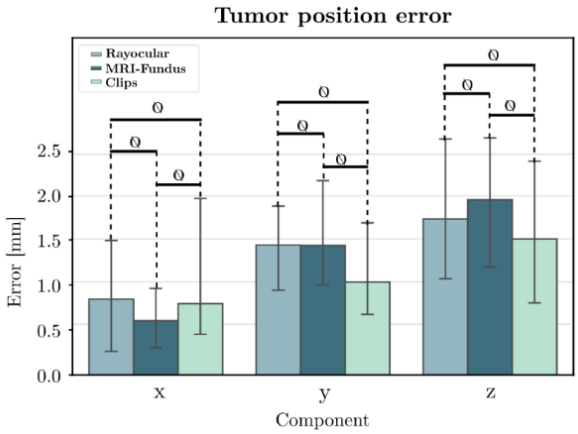

Figure 28. Median and interquartile range of errors in tumour registration using the different kappa angles.

6. DISCUSSION

In ocular proton therapy, the treatment relies heavily on the ability of the patient on fixating on a single point at a predefined position. When the treatment geometry is verified using clips, an estimate of the patient's fixation point is not critical, as clips provide an intraocular geometrical reference which is directly linked to tumour position. On the other hand, clipless eye tracking methods can greatly benefit from an accurate determination of the fixation point to avoid an incorrect estimation of the eye orientation that might lead to significant errors in tumour localisation, especially for posterior targets.

As such, the typically employed assumption that the optical axis is aligned to the visual axis, clearly an oversimplification that leads to mismatches in the real fixation point location, does not stand if clipless eye localization is to be considered.

The hypothesis in this project is that if we accurately model the patient specific deviation between the optical and visual axis (i.e. the kappa angles), one could achieve a more accurate alignment of the tumour position with the planned position using non-invasive eye tracking techniques. In fact, the gaze direction with respect to the optic axis, through this kappa modelling, would be perfectly intersecting the fixation plane at the position of the pre-defined fixation light. As a result, the treatment plan would be adequately delivered to the target position, without the need of radiographic imaging of clips.

In this study, a kappa angles mathematical modelling has been defined as a first step. Its robustness has been validated making use of different sessions, the simulation and the first fraction. The convention is independent from eye orientation changes, as non-significant differences has been observed for the kappa when considering different gaze directions. Our model is also in accordance with values of kappas commonly reported in literature for the left and right eye. This observation is evident in the plot from Figure 24, where the azimuthal components are positive for the right eye and negative for the left eye. Figure 25 further supports this convention, showing that the fovea positions for all patients cluster on the right side of the plot for the left eye and on the left side for the right eye.

Once a strong geometrical modelling of the kappa angle modelling was achieved, a comparison between increasingly patient specific definition of kappas angle values was carried out. Kappa angles were derived from the fovea position defined using the Ray Ocular TPS, the MRI-Fundus registration algorithm presented by Via et al. and, finally, from a clips-based reference fovea estimation.

Results observed in Figure 23, although not quantitatively, illustrate the idea that increasing level of generalization of the fovea (RayOcular model), lead to oversimplification, and therefore higher error in the gaze direction. Higher clustering around 0, and thus lower error in fixation light recalculation is observed from the visual axis estimated by means of the clip-based kappas. This method, however, relies on the assumption that the patient was exactly looking at the fixation light, and the fovea was correctly identified, which was not always the case and most importantly, requires the use of clips. Finally, kappas derived from MRI-fundus image registration while exhibiting sub-optimal results, still in general outperformed the generic kappas used by the RayOcular TPS.

The second part of the study focused on optimising surface registration techniques for non-invasive eye localisation. As hypothesized, increasing number of constraints lead to better convergence of the registration process and ultimately better results.

The method of eye registration based solely on surface-to-surface and pupil minimization constraints, presents with lowest performance in terms of tumour centre of mass localisation with respect to the

reference provided by clips. A possible explanation for this is that the definition of the pupil in the model is a generic approximation, as it was modelled as being on the surface of the cornea. As such, trying to align this estimation of the pupil to the ETS measurement, might lead to suboptimal registration results.

The second method of optimization exhibited better tumour localisation than the previous one, but the overall score is not as good as expected. The reason why this method fails to consistently localize the tumour, is the fact that we are working with angle deviations, and the minimization function might be highly susceptible to fall into local minima. This may explain why in some cases the tumour lies completely off plane while in some others it is the method yielding the best results.

Lastly the third registration method, which is the one with the most complex definition, is examined. The assumption that an increasing number of constraints would lead to better results, is supported by experimental results. In this case, the minimization algorithm is set to optimize the parameters only in a particular direction, one that not only minimizes the angle between optical axes but also constraints the iteratively changing visual axis to lie within the bounds of the patient specific kappa angle. As a result, introducing the kappas as constraints for the visual axis, lead to significant improvement in the tumour centre of mass localization accuracy.

However, which one amongst the three proposed kappa angle estimation methods ultimately provides better registrations when testing the third method, is not clear, see Figure 28. In fact, no significant difference was found in the results when comparing tumour localisation accuracy. Therefore, the hypothesis that clip-based kappas would outperform MRI-Fundus kappas, which would, in turn, outperform Rayocular kappas, is not supported statistically.

A possible explanation for this comes from the choice of the metric used to determine the accuracy of the methods, i.e. the tumour centre of mass. This metric does not adequately capture the complexity of the volumetric model of the tumour. Any type of transformation of this rigid body across the 3 dimensions we are working with, might have shifted the centre of mass significantly with respect to the reference, leading in all cases to suboptimal results. And yet, rotations could compensate translations (and vice versa) and ultimately lead to adequate volume overlaps.

Another point to take into consideration when analysing presented in this study comes from the fact that the sclera in the RayOcular eye model is defined as single structure encompassing its internal and external surface as Figure 29 shows. Since the model sclera is used for the surface-to-surface registration, this ‘double-layer’ effect is certainly affecting the registration accuracy. In fact, based on the lack of specification provided on which layer of the sclera to use for the registration process, the results presented in this study could be furtherly improved.

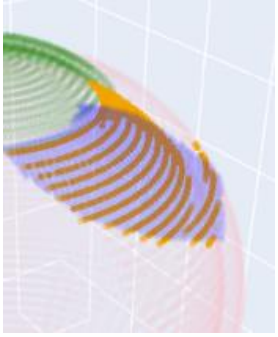

Figure 29. Representation of the double layer of sclera used for surface registration

7. CONCLUSION

The invasive nature of conventional clip-based geometry verification, which heavily depends on practitioner expertise, underscores the need for non-invasive, clipless eye-tracking systems for accurate radiation treatment delivery. This study presents a novel kappa angle model and a robust clipless eye registration method.

Our observations emphasize the relevance of incorporating patient-specific kappa angles into the eye model for precise gaze direction and effective treatment delivery.

Additionally, our findings suggest the need for a more accurate definition of the fovea in eye models, as current methods are either too generic or insufficiently accurate.

8. LIMITATIONS AND FUTURE APPROACHES

This study has several limitations due to its preliminary nature and the complexity of the dataset used, which included a large series of constraints of difficult reproducibility including clip reference positions, MRI acquisitions, pupil tracking, and corneal profilometry. Nonetheless, the small sample size limits the generalizability of the results, necessitating further research with a more diverse set of tumors and patient characteristics.

The methodology for surface registration and performance assessment also had shortcomings. The use of a double-layered sclera model without specifying which layer to refer the registration to, might have led to in some cases, suboptimal eye alignments. Additionally, the simplistic performance metric, based solely on the tumor center of mass, might have introduced errors in evaluating the registration algorithm's true effectiveness, potentially masking the benefits of using clip-based kappas.

Future research should focus on clinical validation of these concepts, testing the efficiency of the clipless method with a more precise definition of fovea position in treatment planning.

BIBLIOGRAPHY

[1] N. V. Laver et M. E. a. D. J. S. McLaughlin, «Ocular melanoma,» 2010.

[2] K. K. Mishra et I. K. Daftari, «Proton therapy for the management of uveal melanoma and other ocular tumors,» 2016.

[3] A. Kacperek, «Protontherapy of eye tumours in the UK: a review of treatment at Clatterbridge,» 2009.

[4] F. Hennings, «Towards a clipless-workflow in Ocular Proton Therapy,» 2018.

[5] J. Hrbacek, K. K. Mishra, A. Kacperek, R. Dendale, C. Nauraye, M. Auger, J. Herault, I. K. Daftari et A. V. a. S. H. A. Trofimov, «Practice patterns analysis of ocular proton therapy centers: the international OPTIC survey,» 2016.

[6] R. Via, A. Fassi, G. Fattori, G. Fontana, A. Pella, B. Tagaste, M. Riboldi, M. Ciocca et R. a. B. G. Orecchia, «Optical eye tracking system for real-time noninvasive tumor localization in external beam radiotherapy,» 2015.

[7] R. Via, F. Hennings, G. Fattori, A. Fassi, A. Pica, A. Lomax, D. C. Weber et G. a. H. J. Baroni, «Noninvasive eye localization in ocular proton therapy through optical eye tracking: A proof of concept,» 2018.

[8] R. Via, K. Bryjova, A. Pica, G. Baroni, A. Lomax, D. C. Weber et G. a. H. J. Fattori, «Multi-camera optical tracking and fringe pattern analysis for eye surface profilometry in ocular proton therapy,» 2023.

[9] J. Wulff, B. Koska, B. Timmermann et M. a. H. J. Janson, «Multimodal imaging in ocular proton therapy treatment planning using RayOcular–first impressions».

[10] R. J. Pumphrey, «The theory of the fovea,» 1948.

[11] R. Via, A. Pica, L. Antonioli, C. Paganelli, G. Fattori, C. Spaccapaniccia, A. Lomax, D. C. Weber et A. a. B. G. Schalenbourg, «MRI and FUNDUS image fusion for improved ocular biometry in Ocular Proton Therapy,» 2022.

[12] T. Haslwanter, «Mathematics of three-dimensional eye rotations,» 1995.

[13] A. Handzel et T. Flash, «The geometry of eye rotations and Listing's law,» 1995.